

**Cooling rates of LL, L and H chondrites and constraints on the duration of peak thermal conditions: Diffusion kinetic modeling and implications for fragmentation of Asteroids and impact resetting of petrologic types**

Jibamitra Ganguly<sup>a,\*</sup>

Massimiliano Tirone<sup>b</sup>

Kenneth Domanik<sup>c</sup>

<sup>a</sup>*Department of Geosciences, University of Arizona, Tucson, AZ 85721, USA*

<sup>b</sup>*Institut für Geologie, Mineralogie, Geophysik, Ruhr-Universität, D-44780 Bochum, Germany*

<sup>c</sup>*Lunar and Planetary Laboratory, University of Arizona, Tucson, AZ 85721, USA*

\*Corresponding author

## 1 **Abstract**

2           We have carried out detailed thermometric and cooling history studies of several LL-, L-  
3 and H-chondrites of petrologic types 5 and 6. Among the selected samples, the low-temperature  
4 cooling of St. Séverin (LL6) has been constrained in an earlier study by thermochronological  
5 data to an average rate of  $\sim 2.6$  °C/My below 500 °C. However, numerical simulations of the  
6 development of Fe-Mg profiles in Opx-Cpx pairs using this cooling rate grossly misfit the  
7 measured compositional profiles. Satisfactory simulation of the latter and low temperature  
8 thermochronological constraints requires a two-stage cooling model with a cooling rate of  $\sim 50$ -  
9 200 °C/ky from the peak metamorphic temperature of  $\sim 875$  °C down to 450 °C, and then  
10 transitioning to very slow cooling with an average rate of  $\sim 2.6$  °C/My. Similar rapid high  
11 temperature cooling rates (200-600 °C/ky) are also required to successfully model the  
12 compositional profiles in the Opx-Cpx pairs in the other samples of L5, L6 chondrites. For the  
13 H-chondrite samples, the low temperature cooling rates were determined earlier to be 10-20  
14 °C/My by metallographic method. As in St. Séverin, these cooling rates grossly misfit the  
15 compositional profiles in the Opx-Cpx pairs. Modeling of these profiles requires very rapid  
16 cooling,  $\sim 200$ -400 °C/ky, from the peak temperatures ( $\sim 810$ -830 °C), transitioning to the  
17 metallographic rates at  $\sim 450$  - 500 °C. We interpret the rapid high temperature cooling rates to  
18 the exposure of the samples to surface or near surface conditions as a result of fragmentation of  
19 the parent body by asteroidal impacts. Using the thermochronological data, the timing of the  
20 presumed impact is constrained to be  $\sim 4555$  – 4560 My before present for St. Séverin (Fig. 3).  
21 We also deduced similar two stage cooling models in earlier studies of H-chondrites and  
22 mesosiderites that could be explained, using the available geochronological data, by impact  
23 induced fragmentation at around the same time. Diffusion kinetic analysis shows that if a lower  
24 petrological type got transformed by the thermal effect of shock impacts to reflect higher  
25 metamorphic temperature, as has been suggested as a possibility, then the peak temperatures  
26 would have had to be sustained for at least 10 ky and 80 ky, respectively, for transformation to  
27 the petrologic types 6 and 4. Finally, we present a model that reconciles textural data supporting  
28 an onion-shell parent body of H-chondrites with rapid cooling rate at high temperature caused by  
29 impact induced disturbance, and also discuss alternatives to the onion shell parent body model.

30

## 1. INTRODUCTION

31 Chondritic meteorites are generally accepted to be the most primitive and  
32 undifferentiated samples of the solar system. The known falls of these meteorites have been  
33 divided into three groups, viz. ordinary chondrites, carbonaceous chondrites and enstatite  
34 chondrites. The ordinary chondrites have been further subdivided into three chemical groups (H,  
35 L and LL) depending on their iron content. The samples in each chemical group are supposed to  
36 have been derived from the same parent body (asteroid) because of the similarity of their  
37 chemical properties (major element chemistry, oxygen isotope ratios) and oxidation state.  
38 Furthermore, samples within a specific chemical group are subdivided into different petrological  
39 types depending on the intensity of metamorphism, as reflected by their peak temperatures  
40 ( $T_{\text{peak}}$ ) deduced from thermometric studies and textural maturity, with the intensity of  
41 metamorphism increasing in the order of the assigned numbers from 3 to 6.

42 It has been suggested, but also strongly debated, as reviewed by Ganguly et al. (2013),  
43 that the parent asteroid of the H-chondrites had an “onion-shell” structure in which each shell  
44 consisted of a specific petrologic type and was enclosed within a shell of lower petrologic type.  
45 This conclusion is based on cooling rates of samples of different petrologic types, as derived  
46 from thermochronological data (age vs. closure temperature relation, mostly below  $\sim 500$  °C with  
47 sufficient spread of data) and their apparent compatibility with the calculated temperature-time  
48 (T-t) paths at different radial distances of an asteroid of 100 km radius, such as those calculated  
49 by Tieloff et al. (2003), Kleine et al. (2008) and Monnereau et al. (2013) (also see review in  
50 Ganguly et al., 2013). The parent asteroid was assumed to have been heated internally by the  $\beta$ -  
51 decay of  $^{26}\text{Al}$  to  $^{26}\text{Mg}$  and cooled by heat conduction (Tieloff et al., 2003; Kleine et al., 2008;  
52 Guignard and Toplis, 2015). Although an onion-shell parent body structure has been suggested  
53 only for H-chondrites, this should be a general feature of a parent body of approximately  
54 spherical shape if it was subjected to internal radiogenic heating with roughly uniform  
55 distribution of heat producing elements.

56 Ganguly et al. (2013) recently carried out a detailed thermometric and cooling rate  
57 studies of selected H chondrite samples on the basis of the compositions of coexisting ortho- and  
58 clino-pyroxenes (Opx and Cpx, respectively) in the metamorphic types 4-6 (H4: Forest Vale; H5:  
59 Allegan and Richardton; H6: Guarena and Kernouvé). They found the compositions of  
60 coexisting pyroxene pairs to be essentially homogeneous within the resolution of an electron  
61 microprobe (Cameca SX-100), and showed that preservation of these profiles requires orders of

62 magnitude faster cooling rates (25-100 °C/ky) at high temperatures, commencing from the  
63 temperatures (750 – 850 °C) reflected by the pyroxene compositions, referred to henceforth as  
64  $T_o$ , than those inferred from the thermochronological constraints at lower temperatures. Ganguly et  
65 al. (2013) thus developed a multistage cooling model that essentially reconciled all constraints on  
66 the cooling rates at both high and low temperatures, including the age vs. closure temperature  
67 ( $T_c$ ) relations, as well as the metallographic cooling rates at intermediate temperatures (~550 °C),  
68 as determined by Krot et al. (2012). However, instead of using conventional  $T_c$  values that  
69 erroneously assume that a specific decay system has a fixed  $T_c$ , Ganguly et al. (2013) calculated  
70 the  $T_c$  values corresponding to the Pb-Pb ages of H chondrites (Göpel et al., 1994) by  
71 considering the effect of grain size, cooling rate and initial temperature at the onset of cooling,  
72 according to the extension of the classic work of Dodson (1973) by Ganguly and Tirone (2001).

73 To explain the very rapid cooling rate at high temperature, Ganguly et al. (2013)  
74 proposed that the parent body of H-chondrites had gone through a history of fragmentation when  
75 much of it was at or near peak temperatures as a result of radiogenic heating; the fragmentation  
76 process caused exposure of samples to surface or near surface conditions, and consequent rapid  
77 cooling. This was followed by reassembly of the fragmented material, thereby leading to slow  
78 cooling of the samples that were buried deeper under a blanket of asteroidal material. All  
79 fragmented material need not have been reassembled into a single secondary parent body, but  
80 some might have accreted to surface of other asteroidal body or gotten mixed with other  
81 asteroidal material to form new rubble pile type asteroids. The discovery of high grade materials  
82 (LL5 and LL6) among the samples scooped from the surface of the asteroid Itokawa (Nakamura  
83 et al., 2011) lends credence to the model of Ganguly et al. (2013).

84 The primary purpose of this work is to extend the pyroxene cooling rate study of Ganguly  
85 et al. (2013) to L, LL and additional samples of H-chondrite samples and see if the results also  
86 reflect a history of fragmentation and reassembly, and if so to determine the timing of the  
87 possible fragmentation episode using available geochronological constraints. These results are  
88 then compared with those of Ganguly et al. (2013) for H-chondrite and two-stage cooling rates of  
89 mesosiderites (Ganguly et al., 1994) to develop a broader understanding of the impact and  
90 cooling histories of asteroidal parent bodies of meteorites, including the timing of the impacts.  
91 We also present constraints, on the basis of diffusion kinetic analysis, on the time period through  
92 which the peak temperatures of type 6 and 4 metamorphic types would have had to be sustained

93 if some of these were produced by impact heating of the lower petrological types that  
94 equilibrated earlier at lower metamorphic temperatures, as suggested by Ciesla et al. (2013) from  
95 impact simulations. Finally, we present an integrated model that attempts to reconcile the  
96 evidence of metamorphism of the asteroidal parent body by internal radiogenic heating with the  
97 cooling rates deduced by Ganguly et al. (2013) and in this study.

## 98 **2. COMPOSITIONAL PROFILES OF COEXISTING ORTHO- AND CLINO-** 99 **PYROXENE PAIRS, THERMOMETRY AND COOLING RATES**

### 100 **2.1. Sample selection and thermometry**

101 We acquired many samples of L and LL chondrites on loan from different sources, but  
102 most of them turned out to be too fine grained, presumably because of shock-induced  
103 brecciation, to be suitable for the present study. The samples with relatively larger grain size that  
104 we selected are as follows: St. Séverin (LL6), ALH 85017 (L6), GRO 85204 (L6) and QUE  
105 90202 (L5), QM USNM 15601 (H6), LAND USNM 6978-1 (H6) (ALH: Alan Hills; GRO:  
106 Grosvenor mountains; QUE: Queen Alexandra range; QM: Queen's Mercy; LD: Landreth Draw;  
107 USNM: United States National Museum). Of these, St. Séverin is of special interest since its  
108 cooling rate below  $\sim 500$  °C has been constrained by geochronological methods (Min et al.,  
109 2013).

110 Recently van Niekerk et al. (2014) have reported results on the peak temperatures of  
111 several H6 and H5 chondrites that include six samples (four H6 and two H5) that were not part  
112 of the set of samples studied by Ganguly et al. (2013). The reported peak temperatures are  
113 comparable to those reported by the latter for H6 and H5 samples using the same thermometric  
114 calibration, and the coexisting clino- and ortho-pyroxene pairs, whose compositions were used to  
115 determine the peak temperatures, have been found to be homogeneous within the resolution of  
116 microprobe analysis. These results imply very rapid high temperature cooling rates, of the order  
117 of  $10^2$  °C/ky, similar to those deduced by Ganguly et al. (2013) for H5 and H6 samples. In this  
118 study, we also selected two more H chondrites, which were not included in the studies of either  
119 Ganguly et al. (2013) or van Niekerk et al. (2014), for detailed thermometric and cooling rate  
120 studies to see if they record any significantly different cooling history that may be compatible  
121 with their metamorphism and *in situ* cooling within an onion-shell parent body.

122 The paucity of clinopyroxene crystals in the chondrite samples made it very difficult to  
123 detect them under optical microscope. Thus, as in Ganguly et al. (2013), we detected coexisting  
124 pairs of Cpx and Opx grains by X-ray mapping in an electron microprobe (Cameca SX100). The  
125 selected pyroxene pairs were then analyzed by step scanning across the interfaces to determine  
126 the compositional profiles of the divalent cations. The conditions for the microprobe analyses are  
127 as follows: 20 kV accelerating voltage, 20 nA beam current with a focused beam of  $\sim 1 \mu\text{m}$   
128 diameter, 20 s counts on the peak and 20 s on the background. Two examples of compositional  
129 profiles, along with the backscattered electron (BSE) images of coexisting pyroxene grains and  
130 traverse lines, are shown in Fig. 1. Special care was taken to ensure that a microprobe traverse  
131 line through an interface did not encounter any fracture or inclusion at or near the interface. For  
132 every sample, we measured almost as many profiles in Opx-Cpx pairs as there are in the thin  
133 section that had clean and fracture free linear segments of interfaces of sufficient lengths so that  
134 traverse lines could be drawn through those segments avoiding the potential problem arising  
135 from interference with the fractures and inclusions and diffusive exchange with the adjacent  
136 minerals. The traverse lines did not deviate by more than a few degrees from normalcy to the  
137 interface and we also ensured that these lines had least interference from fractures or inclusions  
138 within the interior of the crystals.

139 The peak metamorphic temperatures of the samples were determined according to two  
140 formulations: (a) the widely used two-pyroxene (2-Px) thermometric formulation of Anderson et  
141 al. (1993), which is based on extensive experimental studies of Lindsley and co-workers  
142 (Lindsley, 1983 and references therein) on the compositional gap of Ca between Cpx and Opx in  
143 Ca-Fe-Mg-Mn system, and thermodynamic analysis of the data (b) Fe-Mg exchange  
144 thermometry between the two pyroxenes that was formulated by Ganguly et al. (2013) and is  
145 valid when  $X(\text{CaSiO}_3)$  in Cpx  $\geq 0.45$ . For brevity, the formulation (a) will be referred to  
146 henceforth as 2-PX(Ca) and (b) as  $K_D(\text{Fe-Mg})$ . In our judgment, no other 2-PX(Ca) formulation  
147 matches the quality of the one used here because none is based on such an extensive body of  
148 experimental data that demonstrated attainment of equilibrium and rigorous thermodynamic  
149 analysis of the data.

150 We have also considered the thermometric formulations of Brey and Kohler (1990)  
151 which are based on experimental results at 10 – 60 kb in a four-phase lherzolite bulk  
152 composition. The temperatures obtained from  $K_D(\text{Fe-Mg})$  and the formulation based on the

153 transfer reaction  $\text{En}(\text{Opx}) = \text{En}(\text{Opx})$  yield results in two test samples that differed by  $\sim 450$  °C  
154 (633 vs. 1088 °C for St. Séverin; 635 vs. 1073 °C for Landreth Draw). Because of these  
155 discrepancies, we concluded that the formulations of Brey and Kohler (1990) based on the  
156 compositions of coexisting pyroxenes are not suitable at least for the thermometry of the  
157 meteorite samples that requires large extrapolation from the experimental pressure regime,  
158 especially since the correction factor for the pressure effect was not thermodynamically  
159 constrained. There might also have been other problems but a further discussion of the work of  
160 Brey and Kohler (1990) is beyond the scope of this study.

161 The thermometric results are summarized in Table 1 and illustrated in Fig. 2. For each  
162 sample, temperature was estimated for different Opx-Cpx pairs; for each pair, the average  
163 compositions of Cpx and Opx grains were estimated from spot analyses along line scans, such as  
164 illustrated in Fig. 1. For 2-Px(Ca) thermometer the computer program of Anderson et al. (1993)  
165 yields temperature estimates along with their respective  $1\sigma$  errors. Thus, for the 2-Px(Ca)  
166 temperature we present (Table 1 and Fig. 2) the weighted mean temperature for each meteorite  
167 sample along with the standard deviation of the mean (we note, however, that there is very little  
168 difference between the weighted and unweighted means of 2-Px(Ca) temperatures). For the  
169  $K_D(\text{Fe-Mg})$  thermometric results, standard deviations of the means were estimated, using  
170 standard statistical method (e.g. Bevington and Robinson, 2003), by assuming that all  
171 temperature estimates in a given sample have the same standard deviation.

172 There is good agreement between the results from the two thermometric formulations,  
173 except for the samples QM (L6) and QUE (L5), but the temperature calculated from the 2-  
174 Px(Ca) thermometry ( $\sim 825 - 900$  °C) is higher than or almost the same as that from exchange  
175 thermometry ( $\sim 770 - 855$  °C), with an average discrepancy of 33 °C. Ganguly et al. (2013) did  
176 not find any significant difference between the peak temperatures experienced by H5 and H6  
177 samples that they investigated. The same picture also emerges from the data illustrated in Fig. 2.

## 178 **2.2 Determination of cooling rate: method and data**

### 179 *2.2.1 Outline of modeling protocol of compositional profiles in pyroxene diffusion couples*

180 The high temperature cooling rates were calculated on the basis of the thermometric  
181 results and observed compositional profiles of the chosen meteorite samples. For the purpose of  
182 modeling the compositional profiles, we have taken the average of the results from the two

183 thermometric formulations and treated those to be the temperatures that prevailed at the onset of  
184 cooling. These may or may not be the peak temperatures experienced by the sample, but if they  
185 were higher than those recorded by the mineral compositions, then the samples must have been  
186 held long enough at the lower temperatures to achieve compositional homogeneity, as observed,  
187 and cooled subsequently. Resetting of core composition of minerals during cooling leads to  
188 conspicuous zoning from the core to the rim (the compositional difference between core and rim  
189 is what drives resetting of core composition), as demonstrated below, and in other studies, as for  
190 example Ganguly et al. (2013, Fig 6). Thus, since the compositional profiles have been found to  
191 be almost uniform within the resolution of microprobe spot analysis, we assume that the  
192 coexisting pyroxenes were completely homogenized at the onset of cooling from the  
193 temperatures recorded by their compositions.

194         The diffusive exchange of Mg and Fe between coexisting Opx and Cpx has been treated  
195 in terms of a binary inter-diffusion process. The solubility of Ca in Opx is so low ( $\text{Ca} < 1.7\%$  of  
196 the divalent cations) that the effect of Ca on the diffusion of Mg and Fe could be neglected. As  
197 noted by Ganguly et al. (2013), equilibrium Fe-Mg fractionation between the two pyroxenes  
198 during cooling would have caused their Mg/(Mg + Fe) ratio or Mg# at the interface to recede  
199 from one another, and consequently the resulting zoning profiles near the interface would have  
200 been damped in microprobe spot analyses due to spatial averaging or convolution effects, which  
201 depend on the size of the excitation volume within a sample around the center of the electron  
202 beam. The method for correcting for the convolution effect was developed by Ganguly et al.  
203 (1988) and has been incorporated into the numerical code developed by Ganguly et al. (2013),  
204 which is also used in this study for modeling the evolution of compositional profile for  
205 prescribed cooling rate and  $T_0$ . As shown by Ganguly et al. (2013) as well as in the simulations  
206 carried out in this study, convolution correction does not significantly diminish the difference  
207 between profiles that resulted from different cooling rates; for example, profiles developed by  
208 cooling at  $25\text{ }^\circ\text{C/ky}$  is clearly distinguishable from that at  $100\text{ }^\circ\text{C/ky}$  after convolution correction  
209 (Ganguly et al., 2013: Fig. 5). Also convolution of completely homogeneous profiles in two sides  
210 of an interface is typically restricted to  $\sim 1\text{ }\mu\text{m}$  from the interface at the analytical conditions used  
211 in this study, and leads to a decrease in the difference between its true concentrations in the two  
212 sides within this domain (Ganguly et al., 1988: Fig. 4). The details for the two-phase binary  
213 diffusion modeling protocol and mathematical framework have been given in the study of

214 Ganguly et al. (2013). Thus, only a brief and non-mathematical description of the procedure is  
215 given below.

216 Assuming homogeneous initial compositions of both Opx and Cpx, the evolution of  
217 compositional profiles in a coexisting pair was simulated by solving 1-D diffusion equation for a  
218 binary system in Cartesian coordinates. Since diffusion was limited to within a few microns from  
219 the interface, and the traverse lines for microprobe analyses were always much further away  
220 from any grain boundary, 1-D simulation is appropriate. The compositions of the two minerals at  
221 the interface were assumed to satisfy the distribution coefficient of Fe and Mg ( $K_D(\text{Fe-Mg})$ ) as a  
222 function of temperature. An additional boundary condition is imposed by assuming that there is  
223 no interface leaking so that the flux of a component out of one mineral equals that into the other  
224 mineral in a two-pyroxene couple. Since there is no analytical solution to the diffusion problem  
225 that we would be dealing with, a finite difference scheme following the widely used Crank-  
226 Nicolson implicit method (Crank, 1975), which is unconditionally stable, was used to solve the  
227 diffusion equation. The quenched compositional profiles calculated for a prescribed cooling (T-t)  
228 path were then corrected for spatial averaging effect and compared with the measured profiles.  
229 The process was repeated until a satisfactory match was found between the two sets of profiles.

### 230 *2.2.2 Sources of diffusion data*

231 The different sets of diffusion data used in the modeling of concentration profiles in this  
232 study are illustrated in Fig. 3. The primary source of diffusion data are, however, the same as in  
233 Ganguly et al. (2013), namely Zhang et al. (2010) for Cpx and Ganguly and Tazzoli (1994) for  
234 Opx, but with some modifications, as discussed below. The former data set is for diffusion of Mg  
235 instead of the inter-diffusion of Fe and Mg. On the basis of the difference between the available  
236 diffusion coefficients (D) of Fe and Mg in other minerals, Ganguly et al. (2013) argued that use  
237 of D(Mg) for D(Fe-Mg) in Cpx is unlikely to make significant difference in the calculation of  
238 cooling rates. Also, as in their study, we have used D(Mg) data parallel to the b-axial direction  
239 (D(Mg)//b), which, according to Zhang et al. (2010), is the slowest diffusion direction (among  
240 those defined by the crystallographic axes) in Cpx. According to these data, there is very little  
241 difference for diffusion parallel to a and b axial directions, but D(//c) is ~ 5 times greater than  
242 D(//b) at 800 °C, with the difference increasing with decreasing temperature (Fig. 3). The D(Fe-  
243 Mg) in Opx given by Ganguly and Tazzoli (1994) is derived from the data for Fe-Mg order-  
244 disorder kinetics between the M2 and M1 crystallographic sites and, as discussed by them,

245 represent the average of inter-diffusion parallel to the c and b crystallographic axes. We found  
246 that the model fits to the concentration profiles in this study for one sample, St. Severin,  
247 improved if  $D(\text{Fe-Mg})$  of Opx given by Ganguly and Tazzoli (1994) is reduced by a factor of 5;  
248 thus, this adjustment, which is within the uncertainty of the data, was used for all simulations  
249 presented in this study. However, for other samples, there is practically no difference between  
250 cooling rates retrieved from using the modified and original diffusion data for Opx. The use of  
251 the above set of diffusion data should yield roughly a lower bound for the cooling rate required  
252 to produce an observed set of Fe-Mg profiles in a Opx-Cpx pair if the choice of diffusion data is  
253 restricted to Zhang et al. (2010) for Cpx and Ganguly and Tazzoli (1994) for Opx.

254 Dimanov and Wiedenbeck (2006) determined quasi-binary (Fe, Mn)-Mg inter-diffusion  
255 data in natural Cpx as a function of temperature and  $f(\text{O}_2)$  at 1 bar, and presented an Arrhenian  
256 relation at fixed  $f(\text{O}_2)$  of  $10^{-13}$  bars (Fig. 3). However, variation of  $f(\text{O}_2)$  in nature is usually  
257 buffered by mineral assemblages that roughly follows the  $f(\text{O}_2) - T$  relation of a solid oxygen  
258 fugacity buffer like that of iron-wüstite (IW). Thus, and also since  $f(\text{O}_2)$  of chondritic meteorites  
259 is no higher than the latter, we have adjusted the diffusion data of Dimanov and Wiedenbeck  
260 (2006) for variation of  $f(\text{O}_2)$  along the IW buffer with changing temperature according to the  
261 method presented in Posner et al. (2016) and  $\log f(\text{O}_2)$  vs.  $T$  relation for the buffer from O'Neill  
262 (1988). The derived  $\log D$  vs.  $1/T$  relation, which is illustrated in Fig. 3, has the following  
263 Arrhenius parameters:  $D_0 = 3.39(10^{-9}) \text{ cm}^2/\text{s}$  and  $Q$  (activation energy) = 311 kJ/mol.

264 Recently Müller et al. (2014) determined  $D(\text{Fe-Mg})$  in Cpx for diffusion parallel to the c-  
265 axial direction, which is intermediate between those of Zhang et al. (2010) and Dimanov and  
266 Wiedenbeck (2006) parallel to c-axis (Fig. 3). However, in contrast to the latter study, Müller et  
267 al. (2014) did not find any dependence of  $D$  on  $f(\text{O}_2)$ . They explained this on the basis of the fact  
268 that the Cpx crystals used in their diffusion studies are relatively Al rich ( $\text{Al(VI)} = 0.05$ )  
269 compared to those used by Dimanov and Wiedenbeck (2006) ( $\text{Al(VI)} = 0.00$ ). This presumably  
270 led to a nearly constant concentration of octahedral point defects in their Cpx crystals,  
271 irrespective of the variation of  $f(\text{O}_2)$ ; in other words, the extrinsic point defects created by Al  
272 substitution in the octahedral site swamped the variation of point defect concentration resulting  
273 from change of  $f(\text{O}_2)$ .

274 We have considered the effect of variation of the diffusion data for clinopyroxene on the  
275 results of cooling rate retrieved from modeling Opx-Cpx Mg# profiles. This is discussed in the  
276 section 2.3.4.

## 277 **2.3. Results**

278 The results for the modeling of measured compositional profiles of Mg in the Opx-Cpx  
279 pairs in different L, LL and H chondrite samples, along with the available constraints on cooling  
280 rates of some of the samples (St. Séverin: LL6 and H chondrites) from thermochronological and  
281 metallographic studies, are discussed below. For each sample, we have simulated the profile(s)  
282 that showed the least scatter of microprobe data along the chosen traverse across an interface.  
283 However, with regard to the development of zoning near the interface, the measured profiles in a  
284 given sample are very similar.

### 285 *2.3.1. St. Séverin (LL6)*

286 Min et al. (2013) constrained the single grain (U-Th)/He ages from a number of merrillite  
287 and chlorapatite grains separated from St. Séverin (SS). They combined those data with the  
288 Pb/Pb phosphate age (Bouvier et al., 2007), whole rock (WR)  $^{40}\text{Ar}/^{39}\text{Ar}$  ages (Hohenberg et al.,  
289 1981, with revision as discussed by Min et al., 2013) and WR (U-Th)/He ages (Wasson and  
290 Wang, 1991), along with the commonly accepted values for the closure temperatures ( $T_c$ ) for  
291 each decay system, to construct a temperature-time (T-t) path for cooling of St. Séverin below  
292 500 °C. The age vs.  $T_c$  data for the different decay systems, which are illustrated in Fig. 4 by  
293 filled symbols, indicate nonlinear cooling below ~500 °C, with an average rate of ~2.6 °C/My, as  
294 estimated by Min et al. (2013).

295 We have fitted the  $T_c$  vs. age data by a nonlinear cooling function,  $1/T = 1/T_o + \eta t$ , where  
296  $T_o$  is the temperature (K) at the onset of cooling and  $\eta$  is a constant with dimension of  $\text{K}^{-1}\text{t}^{-1}$ .  
297 This cooling model has been used earlier by other workers (e.g. Dodson, 1973; Ganguly, 1982;  
298 Ganguly et al., 2013), and was called an “asymptotic model” by Ganguly (1982). The fitted  
299 relation, which is illustrated in Fig. 3 by a solid red line and corresponds to  $\eta = 6(10^{-6})/\text{K-My}$ ,  
300 has been extrapolated (dashed line) to 875 °C that represents the average of 2-Px(Ca) and  $K_D(\text{Fe-}$   
301  $\text{Mg})$  thermometric results for St. Séverin (Table 1). We note, however, that the extrapolated T-t  
302 path yields an age of 4637 Ma, which is older than the age of the solar system by ~70 Ma. This

303 problem, in itself, is suggestive that the T-t path constrained by the thermochronological data  
304 below  $\sim 500$  °C cannot be extrapolated to the peak temperature.

305 We simulated the evolution of Mg-profiles of Opx-Cpx pairs in St. Séverin as a function  
306 of time, assuming continuous cooling from 875 °C according to the above asymptotic model. The  
307 simulated quenched profiles are compared with the measured data in Fig. 5. It is obvious that  
308 there is a gross mismatch between the simulated and measured profiles, irrespective of the choice  
309 of D(Mg) data for Cpx, that leads us to conclude that the pyroxene profiles could not have  
310 developed by cooling along a T-t path obtained from extrapolation of that constrained by the  
311 geochronological data below  $\sim 500$  °C.

312 To obtain a satisfactory match, as judged by visual inspection, between simulation and  
313 observation, we adopted a two-stage cooling model in which the sample is assumed to have -  
314 cooled rapidly from the peak temperature (875 °C) down to a transition temperature, T(tr), below  
315 which the cooling followed the asymptotic T-t path that is constrained by the geochronological  
316 data (Fig. 4). The results are illustrated in Fig. 6. In each case (also Figs. 7 and 8) the black  
317 dashed lines represent the calculated Mg-profile and the solid red lines represent the convolution  
318 of the calculated profile due to the spatial averaging effect in microprobe spot analyses at the  
319 imposed analytical conditions. The convolved profiles are the ones that should be compared with  
320 the microprobe data.

321 The most successful simulation of the Mg# vs. distance data shown in Fig. 5 is illustrated  
322 in Fig. 5a) for which we used a constant cooling rate (CR) of 200 °C/ky above 450 °C and a  
323 nonlinear T-t path at lower temperature that fits the geochronological constraints (Fig. 4). The  
324 cooling rate at any temperature below 450 °C is given by  $\eta T^2$  with T in Kelvin and  $\eta = 6(10^{-6})$   
325  $/\text{K-My}$ ; thus, at 400 °C,  $\text{CR} = 2.7$  °C/My that is essentially the same as the average cooling rate  
326 (2.6 °C/My) determined by Min et al. (2013). There is a slight misfit between the simulated and  
327 measure concentration profiles on the Opx side of the interface ( $\Delta\text{Mg\#} = 0.013$ ), but we could  
328 not obtain a better match between the two profiles by varying diffusion parameters and initial  
329 temperatures within their permissible limits, and T(tr) (see further discussion in section in  
330 section 2.3.4). We could not obtain an equally satisfactory match between the simulated and  
331 measured profiles, with the former corrected for convolution effect, by setting the transition  
332 temperature (T(tr)) much higher. A simulation with T(tr) = 485 °C, keeping the T-t relation at  
333 higher and lower temperature the same as above, is shown in Fig. 6(b). The quality of fit to the

334 measured Mg-profile did not change by varying the high temperature cooling rate between 200  
335 °C/ky and 800 °C/ky (there is no flexibility for the low temperature T-t path because of the  
336 geochronological constraints). Figure 6(c) shows another successful simulation of Mg profile in  
337 a different Opx-Cpx pair in St. Séverin using the same two-stage cooling model used in the  
338 simulation illustrated in Fig. 6(a).

### 339 2.3.2. L6 and L5 chondrites

340 Selected successful simulations of the measured Mg-profiles in Opx-Cpx pairs in three  
341 L6 and L5 chondrites, GRO (L6), ALH (L6), QUE (L5), are illustrated in Fig. 7 (the  
342 abbreviations of all meteorite names are given in section 2.1 and Table 1). There are good  
343 matches between the measured and the simulated convolved profiles for the following cooling  
344 rates: 200 °C/ky for GRO and ALH and 600 °C/ky for QUE. These simulations do not imply that  
345 the samples cooled at constant rates all through. As in the case of St. Séverin, the cooling rates  
346 could have changed at some low temperatures. If they did, then the transition temperature would  
347 depend on the rate of cooling in the lower temperature regime. For example, if the low  
348 temperature cooling rate was 2.6 °C/ky, similar to the average low temperature cooling rate of St.  
349 Séverin, then the successful simulations of the Mg profiles in the Opx-Cpx pairs in this group of  
350 L5 and L6 samples require the above high temperature cooling rates to continue down to ~450  
351 °C, just as in the case of St. Séverin.

### 352 2.3.3. H chondrites

353 Using metallographic method (central Ni composition of taenite grains following Wood,  
354 1967), Scott et al. (2014) determined the cooling rates of the H chondrite samples, QM (H6) and  
355 LD (H5) to be 20 °C/My and 10 °C/My, respectively. The metallographic cooling rates are,  
356 however, applicable to temperatures around 550 °C. Use of the above cooling rates to model the  
357 Mg profiles of Opx-Cpx pairs in the H chondrite samples, commencing at temperatures recorded  
358 by the pyroxene compositions (QM: ~ 810 °C; LD: ~ 830 °C) lead to quenched Mg profiles that  
359 grossly misfit the measured ones. Accepting the metallographic cooling rates, successful  
360 simulations of the measured Mg profiles of Opx-Cpx pairs require at least a two-stage cooling  
361 model, with ~200 °C/ky for QM and ~400 °C/ky for LD at high temperature and transitioning to  
362 the respective metallographic cooling rates at ~450 °C (Fig. 8). The successful simulations of the  
363 Mg profiles in two Opx-Cpx pairs in QM and LD, using the two-stage cooling models, are  
364 illustrated in Fig. 8. Also shown are profiles with a transition temperature ( $T_{tr}$ ) of 550 °C that

365 fail to match the compositional profiles; variation of high temperature cooling rate does not  
366 improve the match with the observed profiles. To obtain satisfactory match between the  
367 simulated and measured profiles with a  $T(\text{tr}) \sim 550$  °C, the metallographic cooling rates need to  
368 be revised upward by an order of magnitude. However, an equally good match between the  
369 simulated and measured profiles as those illustrated in Fig. 8 with  $T(\text{tr})$  of 450 °C could be  
370 obtained with a  $T(\text{tr})$  of 500 °C if the  $D(\text{Cpx})/b$  is reduced by a factor of 4. As discussed above,  
371 this adjustment of  $D(\text{Cpx})/b$  is within the uncertainty of the experimental data.

372         The two stage cooling model developed above to reconcile the metallographic cooling  
373 rate at low temperature with the orders of magnitude faster cooling rates at high temperature  
374 (constrained by the nearly homogeneous compositions of Opx-Cpx pairs) is qualitatively similar  
375 to that deduced by Ganguly et al. (2013) for Guarena, which is a H6 chondrite. However, in the  
376 latter study, the  $T(\text{tr})$  between the rapid high temperature cooling rate and the much slower  
377 metallographic rate at lower temperature was found to be  $\sim 650$  °C. The substantial difference  
378 between the  $T(\text{tr})$  values of Guarena and the H chondrites studied in this work prompted us to re-  
379 examine the simulations in Ganguly et al. (2013). It was found that in the simulation illustrated  
380 in their Fig. 8, the low temperature metallographic cooling rate was mistakenly entered as 15  
381 °C/ky instead of 15 °C/My. Correcting for this error, we find that the  $T(\text{tr})$  for Guarena is  $\sim 500$ -  
382 550 °C, given the uncertainty of the diffusion data, as discussed above (factor of 4-5), and  
383 allowing for variation of metallographic cooling rate between 15 and 30 °C/My (lowering the  
384 rate of second stage cooling pushes  $T(\text{tr})$  downwards to avoid resetting of the concentration  
385 profiles; the effect of longer time, which favors resetting, is compensated by slower diffusion  
386 kinetics at lower temperature). Thus, the transition temperatures to the slow metallographic  
387 cooling rates of all H5 and H6 samples that we have studied so far fall in the range of  $\sim 500 - 550$   
388 °C.

389         In contrast to the rapid high temperature cooling rates deduced in this study and Ganguly  
390 et al. (2013) for H6 samples (of the order of  $10^2$  °C/ky), the cooling rate in an onion-shell model  
391 at  $\sim 40$  km radial distance, which is considered to be the appropriate location of H6 chondrites in  
392 a spherical parent body of 100 km radius and heated internally by  $^{26}\text{Al}$  decay, is 10-20 °C/My in  
393 the temperature range of 800 – 500 °C (Kleine et al., 2008).

394         2.3.4. *Effect of change of diffusion data and initial conditions on cooling rate calculations*

395 The Fe-Mg diffusion data for Cpx illustrated in Fig. 3 show large variations, which are  
396 due to differences in point defect concentrations, as discussed by Müller et al. (2014), and also  
397 experimental problems including the measurement of the diffusion profiles. We are, however,  
398 not in a position at this stage to analyze the experimental problems associated with the individual  
399 studies. At any rate, we consider here the effect of different sets of diffusion data on the values of  
400 retrieved cooling rates.

401 First, we note that  $D(\text{Fe-Mg})$  of Cpx parallel to the c-axial direction determined by  
402 Müller et al. (2014) is much slower than  $D(\text{Mg})$  determined by Zhang et al. (2010) (Fig. 3). It is,  
403 however, quite close to  $D(\text{Mg})/b$  determined by the latter we used as to model the Opx-Cpx  
404 Mg# profiles (Fig. 6-8). The reason for this discrepancy remains unclear. However, because of  
405 this discrepancy between two data sets for diffusion parallel to the c-axis, we considered the  
406 possibility that  $D(\text{Mg})/b$  in Cpx could be smaller than that given by Zhang et al. (2010), and  
407 tested the effect of lowering the diffusion coefficient by a factor of four on the simulation of a  
408 Mg-profile of a Opx-Cpx pair in St. Séverin and H chondrites. The reduced  $D(\text{Mg})/b$  is a  
409 reasonable lower limit of the data by Zhang et al. (2010), considering the errors of the Arrhenius  
410 parameters of their data. We modeled the Mg# profiles in St. Severin illustrated in Fig. 6(c) with  
411 the adjusted diffusion data for Cpx and found that good match between the simulated and  
412 observed profiles could be obtained, by using high-T cooling rate of 50-200 °C/ky, followed by a  
413 second stage slow non-linear cooling (average 2.6 °C/My) below 450 °C; the quality of  
414 simulation is about the same as illustrated in Fig. 6(c) except that there is a slightly greater  
415 mismatch between the first point from the interface in the Opx side and the simulated Mg#  
416 ( $\Delta\text{Mg\#} = 0.015$ ). The use of the diffusion data of Mueller et al. (2014) yields almost exactly the  
417 same simulated profiles for the same cooling rates as with the  $D(\text{Mg})/b$  data of Zhang et al.  
418 (2010), reduced by a factor of 4.

419 We have tested the effects of reduction of the data of Zhang et al. for  $D(\text{Mg})/b$  by a  
420 factor of 4 and of  $D(\text{Fe-Mg})$  for Opx of Ganguly and Tazzoli (1994) by a factor of 5 for the  
421 simulations in Ganguly et al. (2013). To recapitulate, it has been found in this study that the  
422 downward adjustment for the Opx diffusion data improves the match for the profiles in St.  
423 Séverin (Fig. 6), but other profiles that are essentially flat are insensitive to this change. The Mg#  
424 profiles in Opx-Cpx pairs in the samples studied by Ganguly et al. (2013) have been found to be  
425 insensitive to the adjustment of the diffusion data for Opx, but the downward adjustment for the

426 Cpx data leads to a lowering of cooling rate by a factor of around five from that determined by  
427 Ganguly et al. (2013). This change does not, however, affect any of the conclusions of Ganguly  
428 et al. (2013) since the cooling rates still remain a few orders of magnitude larger than the  
429 available cooling rate data at low temperature cooling. For the Opx-spinel pairs in Ganguly et al.  
430 (2013), the retrieved cooling rates are reduced by a factor of five, i.e. to 10 °C/ky from 50 °C/ky,  
431 if we use the adjusted diffusion data for Opx. Interestingly, the reduced cooling rate is the same  
432 as that determined by Krot et al. (2012) from metallographic data.

433 We have also used the D(Fe-Mg) data of Dimanaov and Wiedenbeck (2006), adjusted for  
434  $f(\text{O}_2)$  variation along IW buffer (Fig. 3) to model the Opx-Cpx Mg# profile of St. Séverin  
435 illustrated in Fig. 6(c). We tried many combinations of high-T cooling rates and T(tr), but could  
436 find a good match, very similar to that shown in Fig. 6(c), to the Mg# profiles of the pyroxenes  
437 only after reducing the D(Fe-Mg) of Opx by a factor of 300 and using a high-T cooling rate of 20  
438 °C/ky along with a T(tr) of 580 °C. The T-t path below the T(tr) is the same as that constrained  
439 by the thermochronological data and used in all simulations of the Opx-Cpx Mg# profiles of St.  
440 Severin.

441 We have also tested the effect of variation of initial temperatures ( $T_0$ ) on the values of  
442 retrieved cooling rates. It should be obvious that increasing  $T_0$  would necessitate faster cooling  
443 rates to produce the same or very similar profiles, since the diffusion coefficients become larger,  
444 and would thus strengthen our model of parent body history based on rapid high-T cooling rates  
445 that we have calculated. Thus, we focus only on testing the effect of lowering  $T_0$  within  
446 permissible limits of the thermometric results. For this exercise, we selected two samples, St.  
447 Séverin and Queen's Mercy. From the thermometric results summarized in Table 1 and  
448 illustrated in Fig. 2, the initial temperatures of these samples could be lowered by no more than  
449 25 °C and 37 °C from the temperatures used in the simulations in Fig. 6 and 8(a). These limiting  
450 values correspond to the temperatures calculated from the  $K_D(\text{Fe-Mg})$  thermometry. The  
451 adjusted temperatures represent, respectively, 43 °C and 75 °C lowering of the temperatures  
452 obtained from the 2-Px(Ca) thermometric formulation (Lindsley, 1983; Anderson et al., 1993)  
453 that were very carefully calibrated, as discussed above, and also has been tested extensively in  
454 studies of terrestrial samples from both metamorphic and igneous rocks. Thus, we do not feel  
455 that any further lowering of the initial temperatures of the sample is justified. The simulations of  
456 the selected profiles using the new initial temperatures yield essentially the same cooling rate as

457 before. In summary, the variation of diffusion parameters and initial temperatures within  
458 permissible limits do not change the overall scenario of very rapid cooling (of the order of  $10 -$   
459  $10^2$  °C/ky) at high temperature.

460

461

### 3. DISCUSSION

462 From the results presented above, it should be obvious that after allowing for the  
463 uncertainties in the diffusion parameters and initial temperatures, modeling of the pyroxene  
464 compositional profiles of all H, L and LL chondrite samples studied so far yield high-T cooling  
465 rates of the order of  $10-10^2$  °C/ky. Göpel et al. (1994) drew attention to the petrographic features  
466 of H chondrites, namely small grain size of ferromagnesian silicates, preservation of  
467 clinobronzite and striated pyroxene, and survival of polycrystalline taenite in H chondrites that,  
468 as emphasized by them, “require a very short time (days or weeks) above 1100 K and fast  
469 cooling” (1100 K is close to the peak temperatures of the samples studied in this work). Use of  
470 low-T cooling rate constrained independently by metallographic methods and/or  
471 thermochronological data to model Mg# profiles in Opx-Cpx pairs grossly misfit the measured  
472 profiles (Fig. 4; Ganguly et al. 2013: Fig. 6). Thus, at least for the samples that show slow low-T  
473 cooling of the order of several to few tens of degrees per My, a two or multi-stage cooling model  
474 is required to fit all constraints on the T-t paths.

475 We discuss below additional implications of the cooling rate studies, temporal constraint  
476 on the feasibility of shock resetting of metamorphic grades, and finally present a synthesis of  
477 cooling rate and textural data of H chondrite to develop a model for metamorphism and shock  
478 history.

#### 479 **3.1. Comparison of the cooling histories of chondrite groups and mesosiderites and** 480 **implications**

481 The rapid high temperature cooling rates (of the order of 200-600 °C/ky) of the L, LL and  
482 H chondrites that we have determined in this study are comparable to the cooling rates deduced  
483 by Ganguly et al. (2013) for H chondrites. In an earlier study on mesosiderites, Ganguly et al  
484 (1994) found that the Fe-Mg profiles in Opx-Opx diffusion couples, which formed in some  
485 samples as a consequence of overgrowth of Opx on earlier formed crystals, imply very rapid  
486 cooling rate,  $\sim 1-10$  °C/ky, from the peak temperature of 1120-1150 °C. These cooling rates are

487 in sharp contrast to the much slower low temperature cooling rates (fraction of a degree to the  
488 order of  $10^2$  °C/My, depending on the temperature) deduced from Ar-Ar ages and corresponding  
489 closure temperature,  $T_c$  (Bogard et al., 1990), metallographic data (Powell, 1969, as modified by  
490 Ganguly et al., 1994) and the quenched Fe-Mg ordering states of orthopyroxenes (Ganguly et al.,  
491 1994). Ganguly et al. (1994), thus, proposed a two-stage cooling model for the mesosiderites  
492 with a transition temperature between 500 °C and 800 °C.

493 Geochronological data provide constraints for the timing of transitions from rapid high  
494 temperature cooling to orders of magnitude slower cooling rate at lower temperatures for the  
495 three groups of meteorites, H, LL and mesosiderites. The T vs. age data for St. Séverin (LL6)  
496 illustrated in Fig. 3 and those for H chondrite (Ganguly et al., 2013, Fig. 11) show that the  
497 transition had taken place ~4555 and 4560 My before present, respectively. The timing for the  
498  $T(tr)$  in the cooling path of the mesosiderites may be constrained from the Sm-Nd mineral ages  
499 ( $4470 \pm 20$  Ma), as determined by Prinzhofer et al. (1992) and interpreted by them to have been  
500 reset by 90 Ma. Sano et al. (2011) showed that this resetting is compatible with that expected  
501 from the cooling model of mesosiderite developed by Ganguly et al. (1994), with all resetting  
502 taking place in the lower temperature slow-cooling limb commencing at ~ 770 °C, since the time  
503 spent by the rock between the  $T_{peak}$  and  $T(tr)$  is too small to cause any significant resetting. Thus,  
504 the timing of the  $T(tr)$  for the mesosiderites becomes 4560 ( $\pm 20$ ) Ma, which is similar to that  
505 deduced for the H and LL chondrites.

506 The rapid high temperature cooling of the H4-6 (Ganguly et al., 2013; this study), L5 and  
507 LL6 samples (this study), as well as mesosiderites (Ganguly et al., 1994), imply exposure of the  
508 samples to surface or near surface conditions. This might have been caused from impact induced  
509 fragmentation of the parent asteroid (Ganguly et al., 2013) or flow of material from the interior  
510 following one or more impacts (Ciesla et al., 2013). The timing of the impacts must have been  
511 only slightly before the  $T(tr)$  of the two-/multi-stage cooling models discussed above since very  
512 little time would have been spent between  $T_o$  and  $T(tr)$  because of the very rapid cooling rate  
513 within this temperature interval. Thus, we conclude that the impacts of the asteroidal parent  
514 bodies of chondrites (LL, L and H) and mesosiderites had taken place between ~4.55 and 4.58  
515 Ga. Although we have not carried out an exhaustive study of the cooling history of meteorites,  
516 we note that numerical simulations of asteroidal impacts by Davison et al. (2013) suggest that  
517 collision rates among asteroids were highest during the first 100 Myr of solar system with a peak

518 activity in the first 5 – 20 Myr. Our results for the timing of the suggested impact induced  
519 disturbance of chondrite (H, L and LL) and mesosiderite parent bodies fall within the period of  
520 peak impact activity suggested by Davison et al. (2013).

### 521 **3.2. Transformation to higher temperature petrologic type by shock effects: constraints on** 522 **the time scale of peak thermal condition**

523 Ciesla et al. (2013) presented simulations of thermal profiles as a function of radial  
524 distance of an asteroid of 100 km radius that formed 2.2 My after CAI formation and was heated  
525 internally by the decay of  $^{26}\text{Al}$  to  $^{26}\text{Mg}$ , and superposed on these the thermal effects of shock by  
526 an impactor 10 My after the formation of the asteroid when the temperature was past the peak  
527 condition but still high (~1200-800 K) at 80-95 km from the center. The impactor was chosen to  
528 be 10 km in diameter colliding with the target at 4 km/s speed. Ciesla et al. (2013) suggested the  
529 possibility that such impact process could have led to the transformation of rocks in the target to  
530 higher petrologic types as a direct result of impact heating and/or burial of pristine crustal rock  
531 under hot rocks exhumed from depths. However, the transformation of petrologic type depends  
532 not only on temperature, but also on the residence time of a rock at the perturbed temperature.  
533 This point was recognized but not addressed by the Ciesla et al. (2013). We provide below  
534 quantitative constraints on the time scale for transformation of petrologic type through diffusion  
535 kinetic modeling.

536 We assume that the thermal effect of an impact instantly resets the surface concentrations  
537 of Opx-Cpx pairs, satisfying the distribution coefficient  $K_D(\text{Fe-Mg})$  at the impact induced  
538 temperature. Cpx grains are rare, and are typically embedded in a matrix in which Opx is a major  
539 component; also all Opx grains in a sample have been found to have essentially the same  
540 composition. Thus, we assume that Opx grains surrounding a Cpx grain had served as a  
541 homogeneous infinite reservoir because of relatively rapid grain boundary diffusion, as  
542 demonstrated experimentally by Liermann and Ganguly (2001). In this case, we can calculate the  
543 minimum time (t) needed to equilibrate the interior of a Cpx grain by assuming a spherical  
544 geometry, for which  $t \sim 0.4(r^2/D)$ , where r is the grain radius (Crank, 1975, Fig. 6.1).

545 We have not determined the orientations of the traverse lines for profile measurements.  
546 However, even if the orientations were known, we do not have adequate diffusion data to  
547 determine the diffusion coefficients parallel to the three principal axes of diffusion (only the b  
548 direction in Cpx constitutes such an axis) that are needed to calculate diffusion coefficient

549 parallel to an arbitrary direction of known orientation. We, thus, use the data for D(Mg) parallel  
550 to the fastest and slowest diffusion directions (c and b axis, respectively) from Zhang et al.  
551 (2010) to calculate the limiting time scales for effectively complete resetting of Mg# in Cpx by  
552 shock induced thermal effect. Taking the data for St. Séverin in Figs. 1 and 2 (also Table 1) for  
553 the grain radius ( $\sim 30 \mu\text{m}$ ) and resetting temperature ( $\sim 870 \text{ }^\circ\text{C}$ ), respectively, we obtain  $\sim 10\text{-}30$   
554 ky for the time scale of resetting of composition of the Cpx grain. If D(Fe-Mg) in Cpx is as slow  
555 as the data of Dimanov and Wiedenbeck (2006) suggest, then the resetting time scale is going to  
556 increase by a factor 17. However, we feel that such a large increase is unlikely because, as  
557 discussed above, use of D(Fe-Mg) data of Dimanov and Wiedenbeck (2006) to model Opx-Cpx  
558 profiles in St. Séverin required an unrealistic lowering of D(Fe-Mg) of Ganguly and Tazzoli  
559 (1994) by a factor of 300.

560 The simulations presented by Ciesla et al. (2013: Fig. 7) do not show the duration of post-  
561 shock peak temperature that could be compared with the results derived above. Their post-shock  
562 T-t paths show very rapid cooling and a transition to very slow cooling at low temperature that  
563 have qualitative similarity with the T-t paths constructed in this study (Figs. 3 & 5) and by  
564 Ganguly et al. (2013: Fig. 11). However, the transition temperatures in the simulations of Ciesla  
565 et al. (2013) are much lower ( $\leq 125 \text{ }^\circ\text{C}$ ) than those deduced from cooling rate studies, which are  
566 in the range of  $450 - 500 \text{ }^\circ\text{C}$ ; also these transition temperatures are inconsistent with the slow  
567 metallographic cooling rates of chondrites ( $10\text{-}20 \text{ }^\circ\text{C/My}$ ) that are valid at  $\sim 550 \text{ }^\circ\text{C}$ , and  
568 thermochronological constraints (Fig 3; Ganguly et al., 2013: Fig. 11) that require initiation of  
569 very slow cooling of chondrites ( $\sim 2 \text{ }^\circ\text{C/My}$ ) at  $\sim 500 \text{ }^\circ\text{C}$ . It remains to be seen if the peak T-t  
570 combination derived above as well as the overall two (or more) stage T-t path deduced in this  
571 study and Ganguly et al. (1994, 2013) could be generated by impact simulations by varying the  
572 model parameters and also considering a wider distribution of samples with respect to the site of  
573 impact. Some of the near surface (within 5 km depth) cooling paths generated by Ciesla et al.  
574 (2013) are similar to those deduced by Ganguly et al. (2013, Fig. 11) for H4 samples, but it is not  
575 clear if the simulated peak thermal conditions are sustained long enough to transform petrologic  
576 type 3 to 4. The time needed for this transformation is even greater than that calculated above for  
577 the sample from St. Séverin because of lower peak temperature of type 4 chondrites. For  
578 example, using the inferred  $T_0$  of Forest Vale H-chondrite of  $\sim 750 \text{ }^\circ\text{C}$  (Ganguly et al., 2013), we  
579 get  $80 - 560 \text{ ky}$  for the transformation of H3 to H4.

### 580 3.3. Towards development of a self-consistent model of the internal structure of the 581 asteroidal parent bodies and their impact and thermal histories

582 It was emphasized by Ganguly et al. (2013) in their study of H chondrites that the rapid  
583 cooling rates at high temperature recorded by the pyroxene compositional profiles are not  
584 incompatible with an onion-shell parent body model at the initial stage; however, the inferred  
585 cooling rates are incompatible with the notion of excavation and delivery of the samples to Earth  
586 from their original sites of metamorphism that was caused by internal radiogenic heating of a  
587 spherical parent body. Subsequently, Scott et al. (2014) also discussed several contradictions of  
588 the age and metal cooling rate data of H-chondrite with the notion of *in situ* cooling in an  
589 undisturbed onion-shell parent body. Furthermore, they have shown that the conformity between  
590 the onion-shell cooling model of H chondrite and the age data of Trieloff et al. (2013) is a  
591 consequence of sampling statistics.

592 If the asteroidal parent bodies of the meteorites became disrupted by impact, then at least  
593 part of the disrupted pieces should be expected to have either gotten (a) accreted to some other  
594 asteroidal bodies or (b) buried under rubble piles on the still intact portion of the parent asteroids.  
595 As discussed by Ganguly et al. (2013), the scenario (a) predicts that higher metamorphic types  
596 (5/6) should be found on the surface of an asteroid, as indeed has been found on the surface of  
597 the asteroid Itokawa (Nakamura et al., 2011). The scenario (b) predicts that different  
598 metamorphic types should show compositional characteristics of both fast (degrees/ky) and slow  
599 (degrees/My) cooling at low temperatures, depending on the post-fragmentation location/burial  
600 depth of the samples. Scott et al. (2014) reported both fast (Forest Vale, Beaver Creek, Ste.  
601 Marguerite:  $\geq 50,000$  °C/My) and very slow (EET86802, GEO etc.: 4 – 60 °C/My)  
602 metallographic cooling rate for H4 through  $\sim 500$  °C. The low-T metal cooling rate for Forest  
603 Vale is quite similar to its high-T cooling rate deduced from Px-profiles by Ganguly et al. (2013)  
604 (also note the possible modification high-T cooling rate in section 2.3.4). The contrasting cooling  
605 rates of H4 differing by several orders of magnitude support the model of fragmentation and  
606 burial under rubble pile scenario (model (b)); however, so far low-T cooling rates of higher  
607 metamorphic types have been found to be very slow, of the order of 10 °C/My.

608 Recently Guignard and Toplis (2015) carried out a detailed study of the textural  
609 properties of iron-rich phases in H-chondrites and found excellent correlation between average  
610 crystal size and the relative depth of the samples that may be inferred on the basis of their

611 metamorphic types and calculated thermal structure in an onion-shell parent body (Monnereau et  
612 al., 2015). This observation would be compatible with our suggestion of parent body disruption  
613 only if the latter had taken place after the peak thermal conditions were attained at different  
614 depths in an onion shell parent body, and no significant grain growth had taken place during  
615 subsequent cooling. To test this hypothesis, we have calculated the extent of grain growth using  
616 the cooling rates of the samples deduced in this work (Figs. 6-8), and the growth equation in  
617 Guignard and Toplis (2015) along with updated kinetic parameters in Guignard et al. (2016), and  
618 indeed found practically no additional grain growth during post-shock cooling of the samples.  
619 Thus, onion-shell parent body model in which metamorphism took place by internal radiogenic  
620 heating may be reconciled with the cooling rates deduced in this study and Ganguly et al. (2013)  
621 if it is assumed that the parent bodies suffered disruption after the peak temperatures were  
622 attained at different depths, i.e. ~10 Ma after CAI formation.

623 An alternative model to what has been presented above is to consider two thermal  
624 episodes, viz. (i) Impact heating of the samples to high temperatures followed by rapid cooling to  
625 the ambient condition, and (ii) a second episode of radiogenic heating and subsequent slow  
626 cooling. In order for such a model to be viable, at least two conditions need to be met:

627 (a) the impact heating must have been sustained for at least 10 ky to set the metamorphic  
628 type and the observed compositional homogeneity of minerals, as discussed in the preceding  
629 section; and

630 (b) the T-t path in the stage (ii) must have been such as not to disturb the compositional  
631 characteristics of the pyroxenes established during the stage (i).

632 As remarked above, the available impact simulation study (Ciesla et al., 2013) did not  
633 provide adequate data to evaluate if the condition (a) could have been satisfied. With respect to  
634 (b), it has been shown, as discussed above, by a number of simulations in this study (Figs. 6 and  
635 8) and in Ganguly et al. (2013) that the transition from rapid high-T cooling rate ( $\sim 10^2$  °C/ky) to  
636 four orders of magnitude slower low-T cooling rate that have been constrained by diffusion  
637 modeling and metallographic methods, respectively, should have taken place at  $\sim 500 - 550$  °C; a  
638 higher transition temperature ( $T(\text{tr})$ ) in the simulations causes disturbance of pyroxene Mg#  
639 profiles (see, for example Fig. 8 in which the Mg# profiles were disturbed even at  $T(\text{tr}) = 550$   
640 °C). The disturbance would be even more in the scenario of post-impact radioactive heating to

641 this temperature range and subsequent slow cooling since there would be some additional  
642 resetting during the prograde limb and peak duration of the T-t path.

643 The restriction of peak temperature to ~550 °C by radiogenic heating would necessitate a  
644 parent body with much lower concentration of heat producing isotopes, especially <sup>26</sup>Al, than has  
645 been commonly assumed since reducing the size of the parent body to limit T(peak) to ~550 °C  
646 may not achieve the slow cooling for H5 and H6 samples deduced from metallographic and  
647 thermochronological data. Additionally, we do not see any way to reconcile the textural data of  
648 Guignard and Toplis (2015) with such a model.

#### 649 ACKNOWLEDGMENTS

650 This research was supported by a NASA grant NNX14AG28G to JG. We are grateful to  
651 the curatorial staffs for meteorite collections of Smithsonian Institution, Johnson Space Center  
652 and Arizona State University for lending the meteorite samples used in this study. Constructive  
653 reviews by Bruce Watson, Fred Ciesla and an anonymous reviewer have led to substantial  
654 improvement of the manuscript. The editorial handling by Mike Toplis that not only involved a  
655 thorough and thoughtful review of the manuscript but also discussions through several e-mail  
656 exchanges is greatly appreciated.

#### 657 REFERENCES

- 658 Anderson D. J., Lindsley D. H. and Davidson P. M. (1993) QUILF: A Pascal program to assess  
659 equilibria among Fe-Mg-Mn-Ti oxides, pyroxenes, olivines and quartz. *Computers &*  
660 *Geosciences* **19**, 1333-1350.
- 661 Bevington P. R. and Robinson O. K. (2003) *Data Reduction and Error Analysis for Physical*  
662 *Sciences*. Mc-Graw Hill, 307 p.
- 663 Bogard D. D., Garrison D. H., Jordan J. L. and Mittlefehldt D. (1990) <sup>39</sup>Ar-<sup>40</sup>Ar dating of  
664 mesosiderites: Evidence for major parent body disruption at 4 Ga. *Geochim. Cosmochim.*  
665 *Acta* **54**. 2549-2564.
- 666 Bouvier A., Blichert-Toft J., Moynier F., Vervoot J. and Albarede F. (2007) Pb-Pb dating  
667 constraints on the accretion and cooling history of chondrites. *Geochim. Cosmochim.*  
668 *Acta* **71**, 1583-1604.
- 669 Brey G. P. and Köhler T. (1990) Geothermobarometry in four-phase lherzolites II. New

- 670 thermobarometers, and practical assessment of existing thermobarometers. *J.Petrol.* **31**,  
671 1353-1378.
- 672 Ciesla F. J., Davison T. J., Collins G. S. and O'Brien D. P. (2013) Thermal consequences of  
673 impacts in the early solar system. *Meteoritics Planet. Sci.* **48**, 2559-2576.
- 674 Crank J. (1975) *The Mathematics of Diffusion*, second ed., Oxford
- 675 Davison T. M., O'Brien D. P., Ciesla F. J. and Collins G. S. (2013) The early impact histories of  
676 meteorite parent bodies. *Meteoritics Planet. Sci.* **48**, 1894-1918.
- 677 Dimanov A. and Wiedenbeck M. (2006) (Fe,Mn)-Mg interdiffusion in natural diopside: effect of  
678  $pO_2$ . *Eur. J. Mineral.* **18**, 705-718.
- 679 Dodson M. H. (1973) Closure temperature in cooling geochronological and petrological systems.  
680 *Contrib. Mineral. Petrol.* **40**, 259-274.
- 681 Ganguly J. (1982) Mg-Fe order-disorder in ferromagnesian silicates II. Thermodynamics,  
682 kinetics and geological applications. In *Advances in Physical Geochemistry*, vol. 2 (ed. S.  
683 K. Saxena), *Advances in Physical Geochemistry*, Springer-Verlag, Berlin, Heidelberg,  
684 New York pp. 58-99
- 685 Ganguly J., Bhattacharya R. N. and Chakraborty S. (1988) Convolution effect on the  
686 determination of compositional profiles and diffusion coefficients by microprobe step  
687 scans. *Amer Mineral* **73**, 901-909.
- 688 Ganguly J. and Tazzoli V. (1994)  $Fe^{2+}$ -Mg interdiffusion in orthopyroxene: Retrieval from the  
689 data on intracrystalline exchange reaction. *Amer Min.* **79**, 930-937.
- 690 Ganguly J., Yang H. and Ghose S. (1994) Thermal history of mesosiderites: Quantitative  
691 constraints from compositional zoning and Fe-Mg ordering in orthopyroxenes. *Geochim.*  
692 *Cosmochim. Acta* **58**, 2711-2723.
- 693 Ganguly J., Tirone, M., Chakraborty S. and Domanik K. (2013) H-chondrite parent asteroid: A  
694 multi-stage cooling, fragmentation and re-accretion history constrained by thermometric  
695 studies, diffusion kinetic modeling and geochronological data. *Geochim. Cosmochim.*  
696 *Acta* **105**, 206-220.
- 697 Göpel C., Manhès G. and Allègre C. (1994) U-Pb systematics of phosphates from equilibrated  
698 ordinary chondrites. *Earth Planet. Sci. Lett.* **121**, 153-171.

- 699 Guignard J. and Toplis M. J. (2015) Textural properties of iron-rich phases in H ordinary  
700 chondrites and quantitative links to the degree of thermal metamorphism. *Geochim.*  
701 *Cosmochim. Acta* **149**, 46-63.
- 702 Guignard J., Toplis, M.J., Bystricky, M., and Monnereau M. (2016). Temperature dependent  
703 grain growth of forsterite–nickel mixtures: Implications for grain growth in two-phase  
704 systems and applications to the H-chondrite parent body. *Earth Planet. Sci. Lett.* **443**, 20-  
705 31.
- 706 Hohenberg C. M., Hudson B., Kennedy B. M. and Podosek F. A. (1981) Noble gas retention  
707 chronologies for the St. Séverin meteorite. *Geochim. Cosmochim. Acta* **45**, 535-546.
- 708 Kleine T. A., Touboul M., Van Orman J. A., Bourdon M., Maden C., Mezger K. and Halliday A.  
709 N. (2008) Hf-W thermochronometry: Closure temperatures and constraints on the  
710 accretion cooling history of H chondrite parent body. *Earth Planet. Sci. Lett.* **270**, 106-  
711 118.
- 712 Krot T. A, Goldstein, J. J., Scott E. R. D., Wakita S. (2012) Thermal histories of H3-H6  
713 chondrites and their parent asteroid from metallographic cooling rates and cloudy taenite  
714 dimensions. Meteoritical Society Meeting # 5372 (abstr.)
- 715 Liermann H-P. and Ganguly J. (2001) Compositional properties of coexisting orthopyroxene and  
716 spinel in some Antarctic diogenites: Implications for thermal history. *Meteor. Planet. Sci.*  
717 **36**, 155-166.
- 718 Min K., Reiners P. W. and Shuster D. L. (2013) (U-Th)/He ages of phosphates from St. Séverin  
719 LL6 chondrite. *Geochim. Cosmochim. Acta* **100**, 282-296.
- 720 Monnereau M., Toplis M. J., Baratoux D. and Guignard J. (2013) Thermal history of the H-  
721 chondrite parent body: Implications for metamorphic grade and accretionary time-scales.  
722 *Geochim. Cosmochim. Acta* **119**, 302-321.
- 723 Müller T., Dohmen R., Becker H-W., ter Heege J. H. and Chakraborty S. (2015) Fe-Mg  
724 interdiffusion rates in clinopyroxene: experimental data and implications for Fe-Mg  
725 exchange thermometers. *Contrib. Mineral. Petrol.* **166**, 1563-1576.
- 726 Nakamura T., Noguchi T., Tanaka M., Zolensky M.E., Tsuchiyama M. A., Nakato A., Ogami T.,  
727 Ishida H., Uesugi M. Fujimura A., Okazaki R., Sandford S. A., Ishibashi Y., Abe M.,  
728 Ueno M., Mukai T., Yoshikawa M., and Kawaguchi J. (2011) Itokawa Dust Particles: A

- 729 Direct Link Between S-Type Aste Ordinary Chondrites. *Science* **333**, 1113-1116. O'Neill  
730 H. St. C. (1988) Systems Fe-O and Cu-O: Thermodynamic data for the equilibria Fe-  
731 "FeO", Fe-Fe<sub>3</sub>O<sub>4</sub>, "FeO"-Fe<sub>3</sub>O<sub>4</sub>, Cu-Cu<sub>2</sub>O from emf measurements. *Amer. Min.* **73**, 470-  
732 486.
- 733 Powell B. N. (1969) Petrology and chemistry of mesosiderites I. Textures and compositions of  
734 nickel-iron. *Geochim. Cosmochim. Acta* **33**, 789-810.
- 735 Prinzhofer A., Papanastassiou D. A. and Wasserburg G. J. (1992) Samarium-neodymium  
736 evolution of meteorites. *Geochim. Cosmochim. Acta* **56**, 797-815.
- 737 Sano J., Ganguly J. and Hervig R. and Dohmen R. (2011) Neodymium diffusion in  
738 orthopyroxene: Experimental study problemies and applications to geological and  
739 planetary problems. *Geochim. Cosmochim. Acta* **75**, 4684-4698.
- 740 Scott E. R. D., Krot T. V., Goldstein J. I. and Wakita S. (2014) Thermal and impact history of H  
741 chondrite parent asteroid during metamorphism: Constraints from metallic Fe-Ni.  
742 *Geochim. Cosmochim. Acta* **136**, 13-37.
- 743 Trieloff M., Jesserberger E. K., Herrwerth I., Hopp J., Fiénel C., Ghélls M., Bourot-Denise M.  
744 and Pellas P. (2003) Structure and thermla history of H-chondrite parent asteroid revealed  
745 by thermochronometry. *Nature* **422**, 502-506.
- 746 van Niekerk D., Scott E. R. D. and Taylor J. (2014) Constraints on the thermal and impact  
747 history of ordinary chondrites from two-pyroxene equilibration temperatures. 48 th *Lunar*  
748 *Planet. Sci. Conf.* #2374 (abstr.).
- 749 Wasson J. T. and Wang S. (1991) The histories of ordinary chondrite parent bodies. U, Th-He  
750 age distributions. *Meteoritics* **26**, 161-167.
- 751 Wood J. A. (1967) Chondrites: their metallic minerals, thermal histories and parent planets.  
752 *Icarus* **6**, 1-49.
- 753 Zhang X., Ganguly J. and Ito M. (2010) Ca-Mg diffusion in diopside: tracer and chmical inter-  
754 diffusion coefficients. *Contrib. Mineral. Petrol.*, **150**, 175-186.

755 Table 1.

756 Summary of thermometric results cooling rates for L-, LL-, and H-chondrites. Parenthetical  
757 numbers represent standard deviations of the estimated mean temperatures.

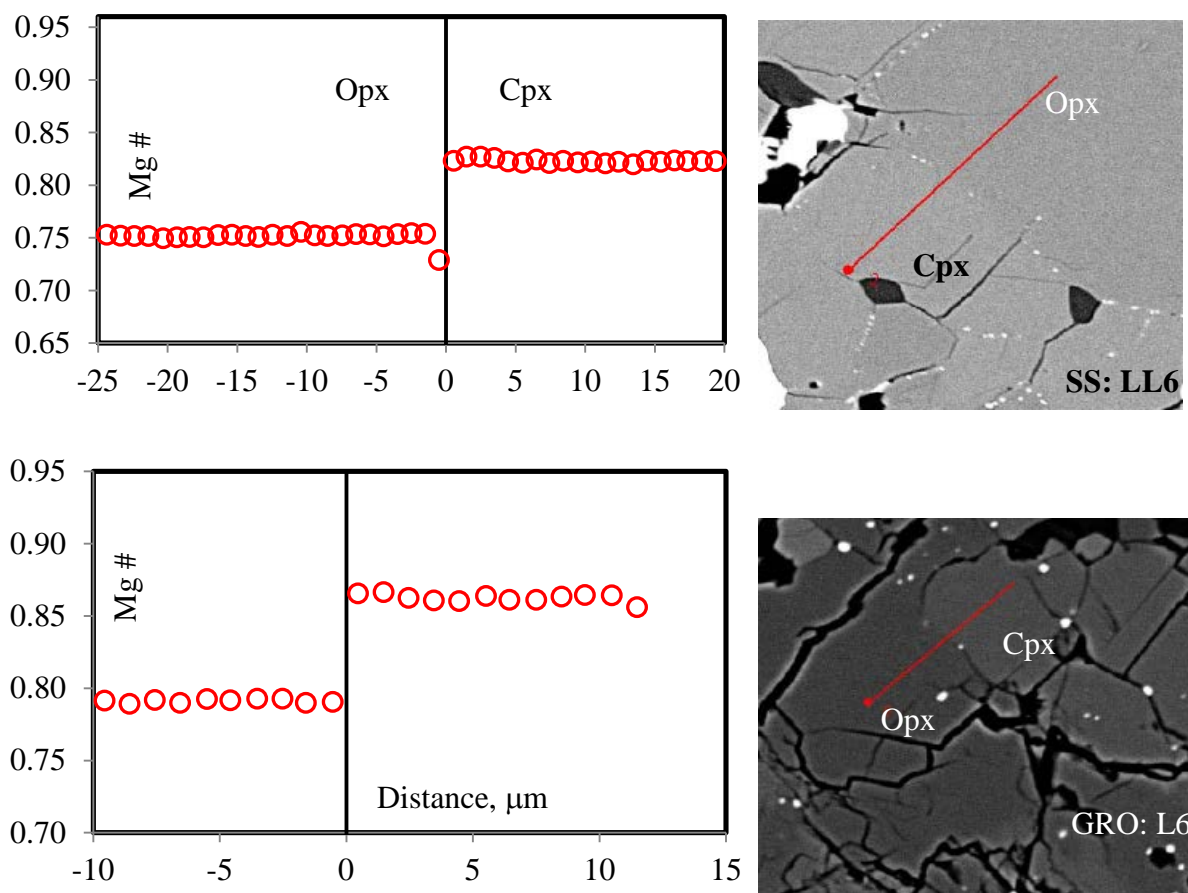
758 -----

Meteorite	Type	$T, ^\circ\text{C}$ (mean)		Average cooling rate	
		2-Px (Ca)	$K_D(\text{Fe-Mg})$	High Temp.	Low Temp.
St. Séverin	LL6	883 (9)	855 (11)	200 $^\circ\text{C}/\text{ky}^*$	2.6 $^\circ\text{C}/\text{My}$ ( $T_{\text{tr}} \sim 450^\circ\text{C}$ )
ALH 76001	L6	868 (9)	844 (21)	200 $^\circ\text{C}/\text{ky}$	
GRO 90202	L6	839 (9)	833 (8)	200 $^\circ\text{C}/\text{ky}$	
QUE 90202	L5	903 (23)	843 (2)	600 $^\circ\text{C}/\text{ky}$	
QM	H6	845 (15)	771 (5)	200 $^\circ\text{C}/\text{ky}$	10 $^\circ\text{C}/\text{My}$ ( $T_{\text{tr}} \sim 450\text{-}500^\circ\text{C}$ )
LD	H5	824 (5)	831 (4)	400 $^\circ\text{C}/\text{ky}$	20 $^\circ\text{C}/\text{My}$ ( $T_{\text{tr}} \sim 450\text{-}500^\circ\text{C}$ )

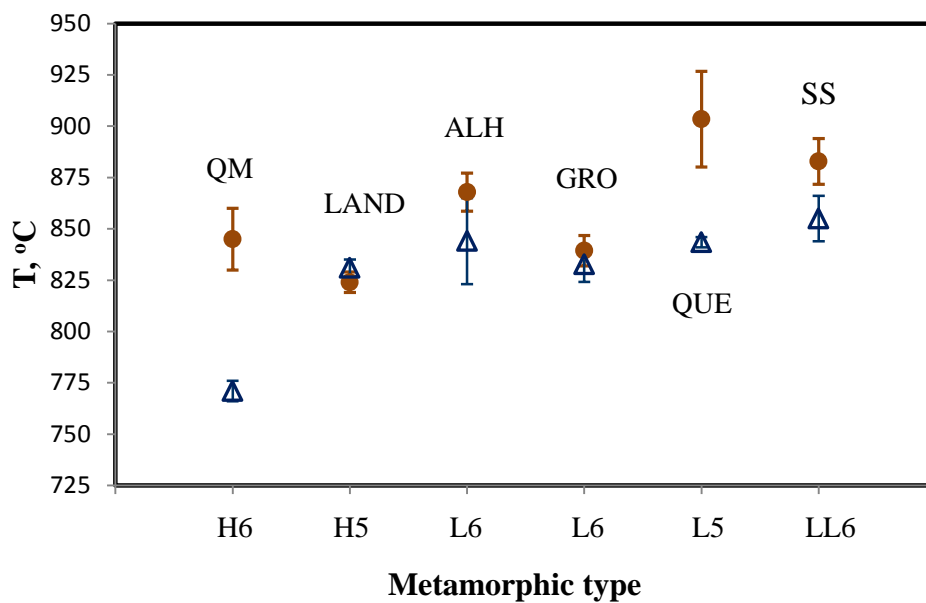
762 -----

770 ALH: Allan Hills; GRO: Grosvenor Mountains; QUE: Queen Alexandra Range; QM: Queen's  
771 Mercy; LD: Landreth Draw.  $T_{\text{tr}}$ : transition temperature.

772 \*A factor of ten reduction is possible considering the full range of diffusion data for  
773 clinopyroxene.



774 Fig. 1. Two representative profiles for Mg/(Mg + Fe) ratio (Mg#) in coexisting ortho- and clino-  
 775 pyroxene (Opx-Cpx) pairs. The 2-Px pairs are in St. Séverin (SS: LL6) and Grossvenor  
 776 Mountains (GRO: L6) meteorites. The backscattered electron images and traverse lines (red  
 777 lines) corresponding to the profiles are shown on the right. The scale can be judged from the  
 778 length of a profile on the left and that for a traverse on the BSE images (20  $\mu\text{m}$  and 11.5  $\mu\text{m}$  in  
 779 the Cpx side of St. Séverin and GRO, respectively).



780 Fig. 2. Mean temperature vs. petrologic type of different H, L and LL chondrite samples  
 781 according to 2-Px(Ca) (filled circles) and Fe-Mg exchange (open triangles) thermometers. The  
 782 vertical error bars show the standard deviations of the means.

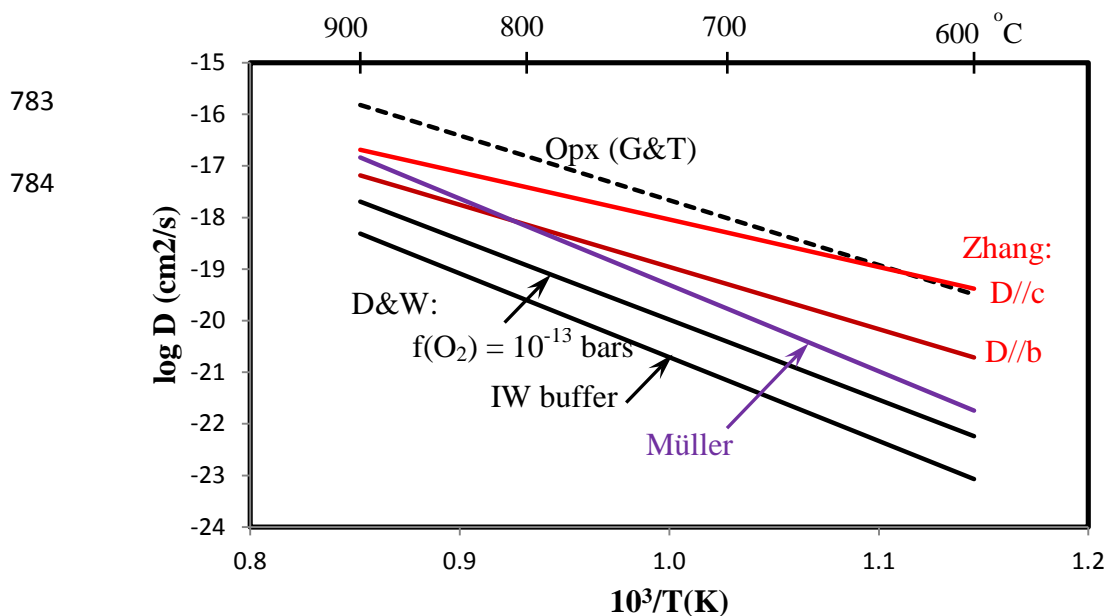
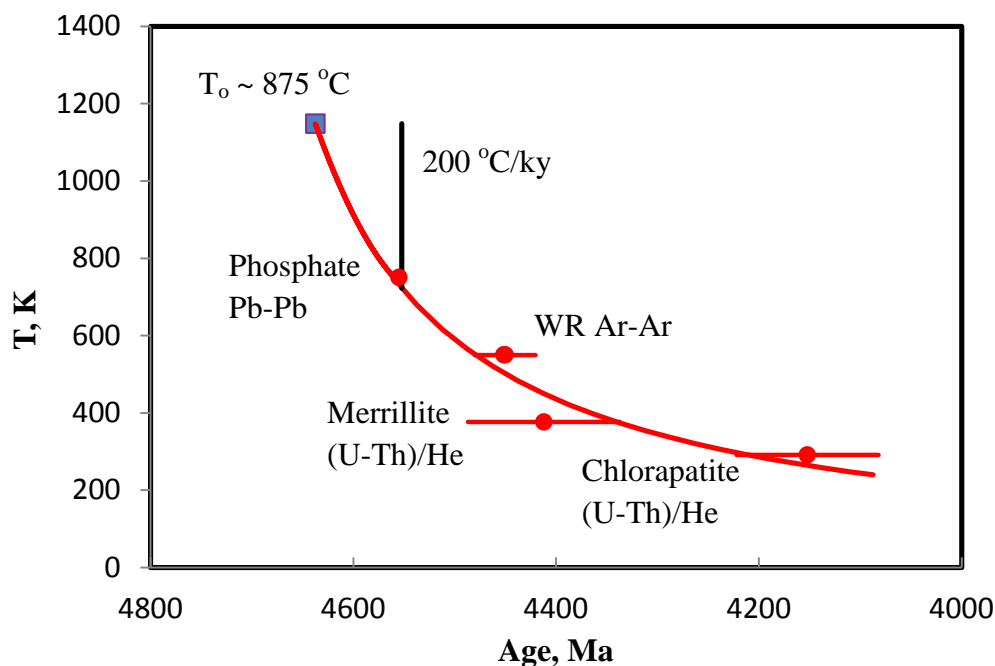


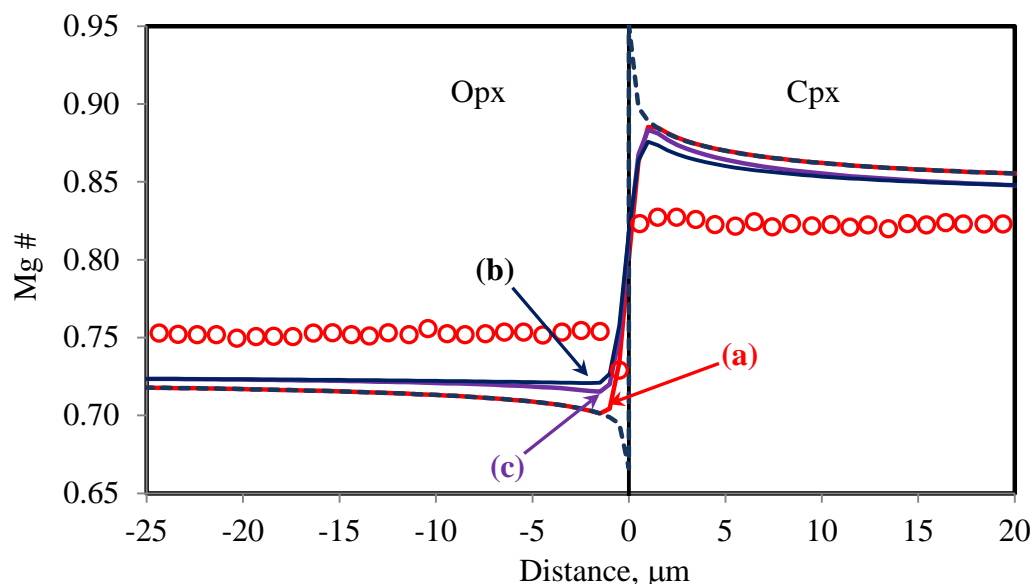
Fig. 3. Summary of diffusion used in modeling Mg# profiles in Opx-Cpx pairs. All solid lines represent diffusion data for clinopyroxene (Cpx) whereas the dashed line represents the  $D(\text{Fe-Mg})$  data of Ganguly and Tazzoli (1994) in orthopyroxene, averaged for diffusion parallel to c and b axial directions. The explanation for Cpx diffusion data is as follows; solid red:  $D(\text{Mg})//b$  and  $D(\text{Mg})//c$  (upper and lower lines, respectively) of Zhang et al. (2010); violet:  $D(\text{Fe-Mg})//c$  of Müller et al. (2015); black:  $D((\text{Fe,Mn})\text{-Mg})$  of Dimanov and Wiedenbeck (2006) at  $f(\text{O}_2) = 10^{-13}$  bars (upper line) and corrected for  $f(\text{O}_2)$  variation with T along IW buffer (lower line).

785

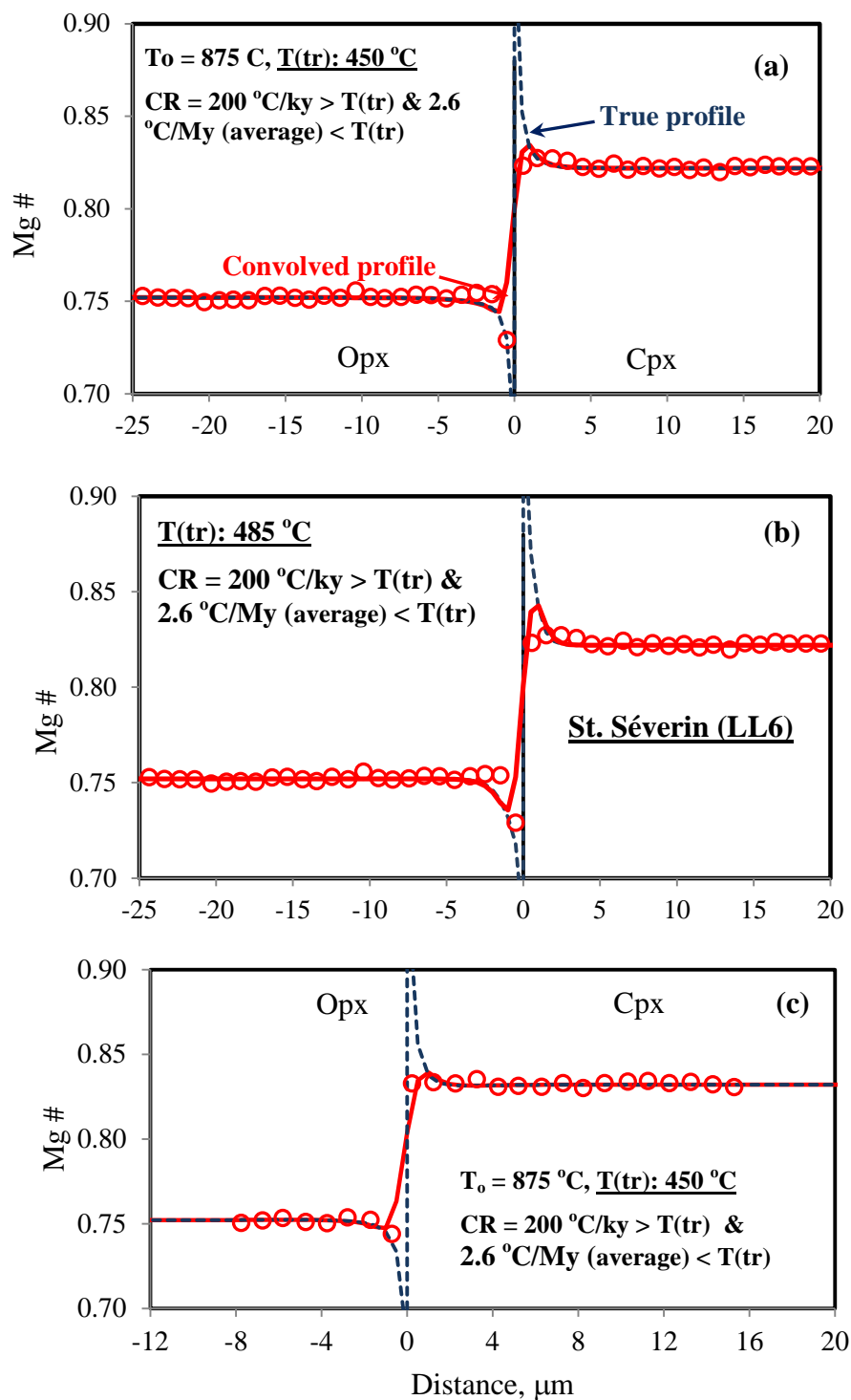


786

787 Fig. 4. Thermochronological data ( $T_c$  vs. age: filled red circles) for St. Séverin as summarized by  
 788 Min et al. (2013). The original sources of the data and uncertainty of the ages (in My) are as  
 789 follows: Phosphate (Bouvier et al., 2007;  $\pm 0.1$ ); Ar-Ar (Hohenberg et al., 1981,  $\pm 30$ ); Merrillite  
 790 (Min et al., 2013; 75); Chalcopyrite (Min et al., 2013; 70). The data have been fitted by an  
 791 asymptotic cooling model (solid red line),  $1/T(K) = 1/T_o(K) + \eta t$ , with  $\eta = 6(10^{-6})/K\text{-My}$ , and  
 792 extrapolated to the peak temperature, 875 °C, as estimated in this study (Table 1). The nearly  
 793 vertical line (black) shows the high temperature segment of the two-stage cooling model needed  
 794 for the successful simulation of the compositional profiles in Opx-Cpx pairs, preserving the  
 795 geochronological constraints.

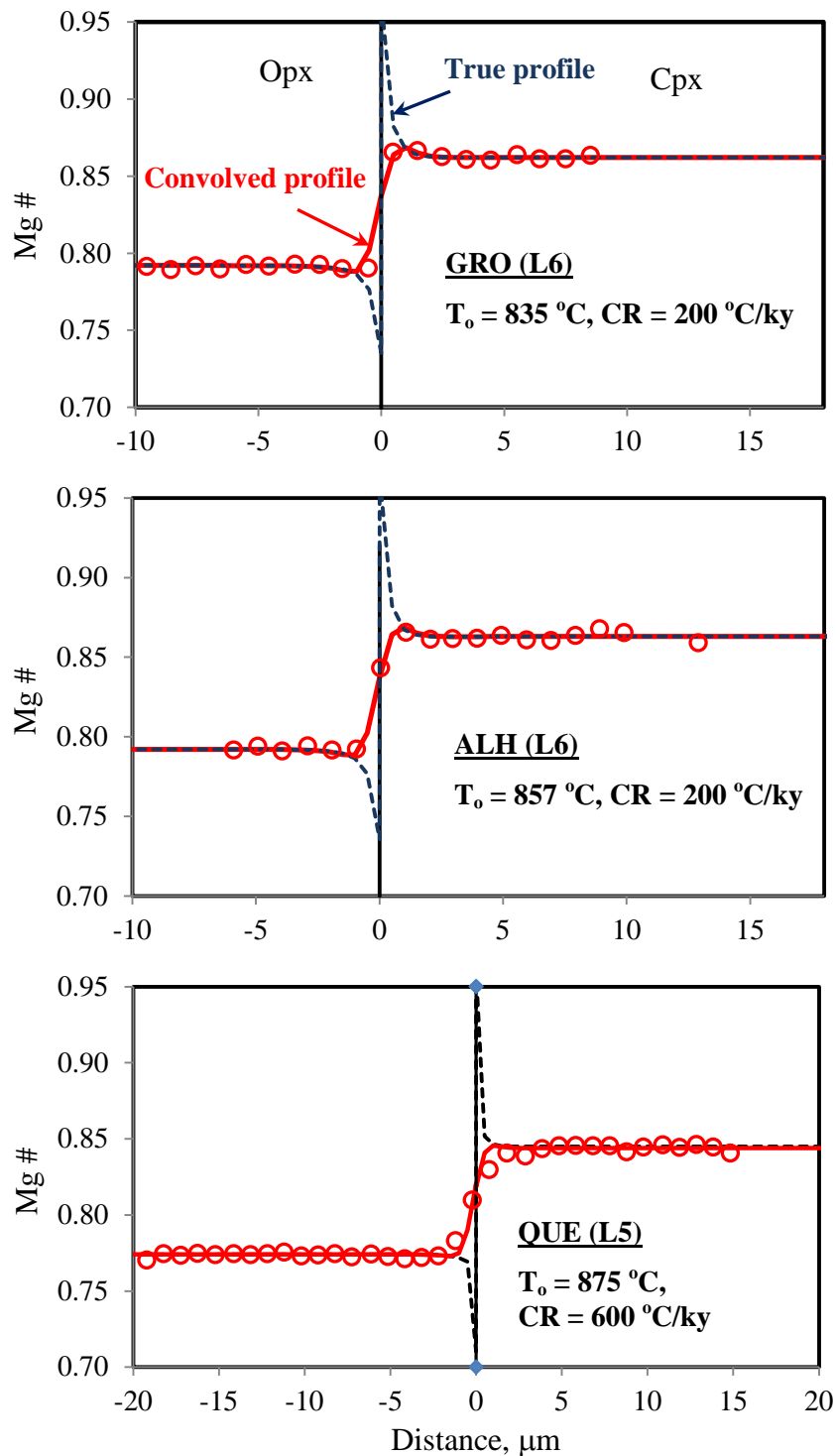


796 Fig. 5. Comparison of the measured Mg# data vs. distance (open circles) in Opx-Cpx pair in St.  
 797 Séverin (LL6) with those developed as quenched profiles in numerical simulations using an  
 798 asymptotic cooling model,  $1/T = 1/T_0 + \eta t$ , with  $\eta = 6(10^{-6}/\text{K-My})$ , which is derived from the  
 799 low-temperature ( $< 500\text{ }^\circ\text{C}$ ) thermochronological data (Fig. 3). In all simulations,  $D(\text{Fe-Mg})$  for  
 800 for Opx is from Ganguly and Tazzoli (1994), reduced by a factor of 5 whereas three sets of  
 801 diffusion data have been used for Cpx (as discussed in the text). Dashed line: simulated profile  
 802 using  $D(\text{Mg})/b$  of Cpx from Zhang et al. (2010), whereas the solid red line (a) is the calculated  
 803 convolution of the simulated profile due to the spatial averaging effect in microprobe spot  
 804 analyses. The two other solid lines are also convolved quenched profiles corresponding to  
 805 different diffusion data for Cpx: (b)  $D(\text{Fe-Mg})/c$  by Müller et al. (2014) and (c)  $D(\text{Mg})/b$  from  
 806 Zhang et al (2010), reduced by a factor of 4.

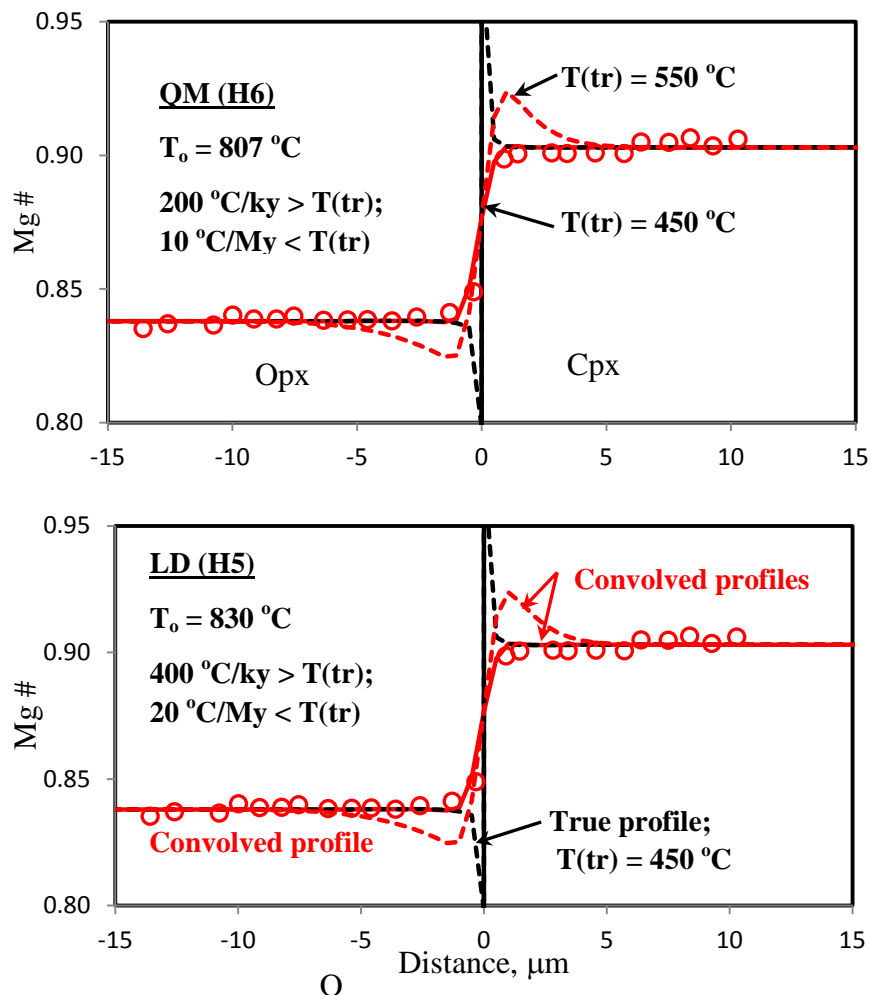


807 Fig. 6. Numerical simulation of the development of compositional profiles in Opx-Cpx pairs in  
 808 two Opx-Cpx pairs in St. Séverin (LL6) by two stage cooling process with two different  
 809 transition temperatures: 450  $^\circ\text{C}$  for (a) and (c) and 485  $^\circ\text{C}$  for (b); the second stage cooling  
 810 follows the thermochronologically constrained nonlinear T-t path illustrated in Fig. 4. Dashed

811 line: simulation (final true profile), solid line: calculated convolution of the simulated profile  
812 accounting for the spatial averaging effect in microprobe analyses. A range of simulations have  
813 been carried out to find the best match to the Mg# vs. distance data (open circles) for each  
814 sample. The measured profiles in (a) and (b) are the same; the traverse line is shown in the BSE  
815 image in Fig. 1 (SS: LL6).



816 Fig. 7. Successful simulations of compositional profiles (Mg#) in L6 and L5 chondrites with  $T_0$   
 817 (constrained by thermometry) and cooling rates indicated in the panels. For a change of cooling  
 818 rate at low temperature of  $2.6 \text{ }^\circ\text{C/ky}$ , as in St. Séverin (LL6, Fig. 6), the high temperature cooling  
 819 rates of the samples would have to continue down to  $450 \text{ }^\circ\text{C}$ .



820 Fig. 8. Numerical simulations of compositional profiles (Mg#) in H6 and H5 chondrites with  
 821 two-stage cooling models. Convolved profiles with transition temperature of 450 °C and 550 °C  
 822 are indicated by solid and dashed red lines, respectively. The low temperature cooling rates are  
 823 constrained by metallographic data.

